Lecture 5: Thin Airfoil Theory

Aerodynamics

Aniruddha Sinha

Department of Aerospace Engineering, IIT Bombay

We are interested in the prediction of lift on an airfoil in an analytical manner. That is, we seek a closed-form expression for the lift, with as little recourse to numerical calculations as possible. Of course, this imposes some restrictions on the validity of the analysis – viz. to thin airfoils at low angles of attack. The significant advantage is the unparalleled analytical insight that it affords as a conceptual model. The theory was first expounded by Glauert.

The thin airfoil theory developed here is valid for two-dimensional, incompressible, steady flow over a thin airfoil at a sufficiently high Reynolds number such that the boundary layer is thin. We have already seen sufficient justification for pursuing potential flow theory for predicting the lift and pitching moment on an airfoil under these conditions.

We have made the following observations in our discussion of potential flow theory, all of which we will leverage in the ensuing derivation:

- The freestream approaching an airfoil is readily simulated by a uniform flow.
- There is no lift without circulation around the airfoil.
- The only way to simulate circulation in the context of potential flow theory is to have irrotational line vortices (distributed within the boundary of a solid body).
- The displacement effect on streamlines around an immersed body (having a closed curve for a boundary) can be simulated by arraying sources and sinks of zero net strength (within the boundary of the body).

In thin airfoil theory, we make the following assumptions:

- The airfoil is thin,
- The camber is small, and
- The angle-of-attack is small.

The upshot of these assumptions is that the airfoil does not disturb or perturb the flow significantly. In particular, disturbances vanish far enough away from the airfoil.

1 Characterizing the airfoil shape

A general airfoil is shown in figure 1. We choose the leading edge as the origin of the coordinate system, $x-$axis along the chord from leading edge to trailing edge (later we will relax this constraint to gain flexibility in modelling), and $z-$axis normal to the $x-$axis directed from the pressure surface towards the suction surface.

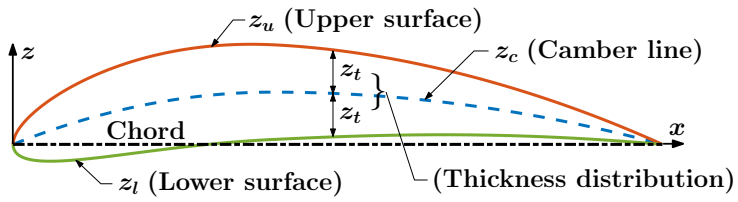

Figure 1: Airfoil shape functions

The upper and lower (respectively the suction and pressure) surfaces of the airfoil are characterized by the shape functions $z_u(x)$ and $z_l(x)$, respectively. We define the functions

$$\text{Camber function:} \qquad z_c(x) := \frac{z_u(x) + z_l(x)}{2},$$

$$\text{Thickness function:} \qquad z_t(x) := \frac{z_u(x) - z_l(x)}{2}.$$

The thickness function always evaluates to a positive value. This is not necessarily the case for the camber function (think of negatively cambered airfoil).

Evidently, the camber function defines the camber line that is the locus of points midway between the upper and lower surfaces (measured normal to the x-axis). As a consequence of the above definitions, we also have

$$\text{Upper surface:} \qquad z_u(x) = z_c(x) + z_t(x),$$

$$\text{Upper surface:} \qquad z_l(x) = z_c(x) - z_t(x).$$

In the following developments, we will assume that the camber and thickness distributions are known, and we will use these latter pair of equations to characterize the geometry of the airfoil surfaces.

2 Kutta condition

The application of potential flow theory to prediction of airfoil lift and pitching moment runs into a fundamental paradox: circulation around the airfoil is required to produce lift (Kutta-Joukowski theorem), but the unique amount of circulation required to simulate the flow around an airfoil cannot be determined from the theory. An indication of this issue could be found in the discussion of simulation of flow around a rotating cylinder using potential flow theory. The theory admitted infinitely many solutions for the arbitrary choice of the circulation (i.e., the strength of the line irrotational vortex ingredient), and there was no unique way of determining this from the theory alone.

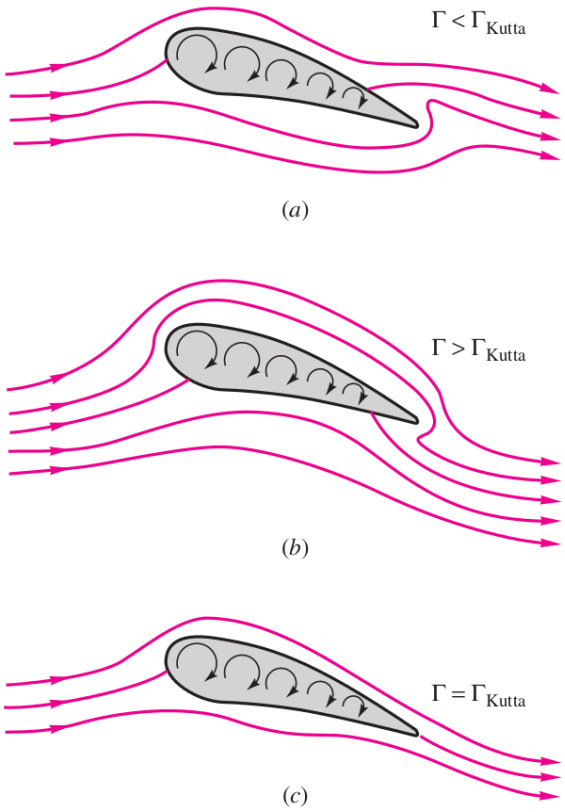

Figure 2: Motivation for Kutta condition [White, F. M., *Fluid Mechanics*, McGraw-Hill, 2009]

Consider now three possible flow solutions around a lifting airfoil predicted by potential flow theory, as shown in figure 2. Solution (a) has the least circulation, such that the rear stagnation point is on the upper surface. Solution (b) has the highest circulation, and the rear stagnation point is now on the lower surface. Solution (c) has an intermediate circulation that is just sufficient for the rear stagnation point to coincide with the trailing edge.

In all but the last potential flow solution, the (inviscid) potential flow predicts an unphysical flow turning around the sharp trailing edge that in reality would cause viscous flow separation due to the severe adverse pressure gradient. This is well substantiated by all experimental observations; see for example figure 3. Thus, Kutta proposed the following additional heuristic condition on potential flow solutions in case of airfoils with a sharp trailing edge: the circulation should be just sufficient so that the flow leaves the trailing edge smoothly. This is an ad hoc (albeit highly effective) way of incorporating viscous effects in the otherwise inviscid potential flow solution. The Kutta condition, as the potential flow theory, only applies if the flow is attached till the trailing edge.

Let us analyze the mathematical implication of the Kutta condition with the help of the schematic shown in figure 4. If the flow is to leave the trailing edge smoothly in agreement with the Kutta condition, the upper and lower surface flow velocities must be tangential to the respective surfaces at the trailing edge. For a sharp trailing edge, there are only two geometric possibilities: (a) the finite-angle or wedge TE or (b) the cusped TE. A finite-angle

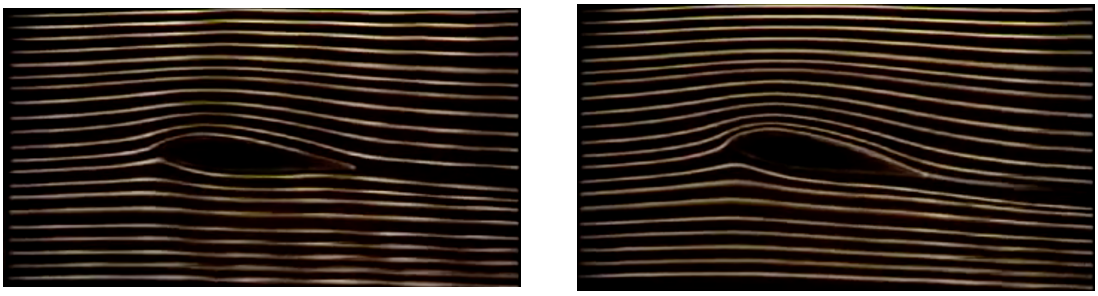

(a) At a small angle of attack (b) At a higher angle of attack

Figure 3: Flow leaving the trailing edge smoothly in two stills from Prof. Babinsky's video.

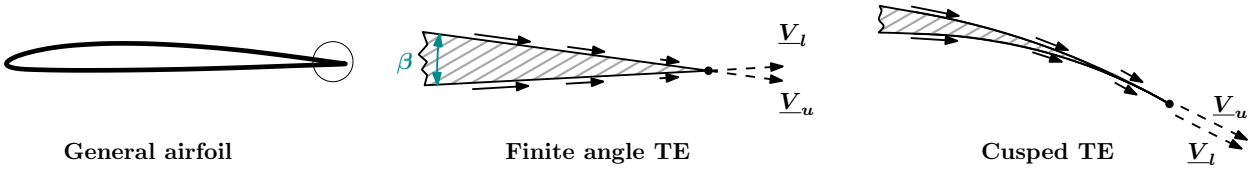

Figure 4: Setup for deriving mathematical statement of Kutta condition.

TE is created if the upper and lower surfaces have different tangents where they meet at the trailing edge. On the other hand, if the two surfaces have the same tangent at their point of intersection, we obtain a cusped trailing edge, as shown in the figure.

In case of the finite-angle TE, figure 4 indicates that we apparently have two different velocities at the trailing edge. But such intersection of streamlines is not possible, unless the intersection were a stagnation point. Thus, we conclude that for a finite-angle TE, $V_u|_{TE} = V_l|_{TE} = 0$, where $V := |\underline{V}|$.

In case of the cusped trailing edge, we take a different approach. We note that the static pressure must be the same on both the upper surface and lower surface streamlines where they come together at the trailing edge. Otherwise, there will be a net unbalanced force on fluid particles in the vicinity which will disturb the steady flow. In case of *incompressible* and *irrotational* flow, Bernoulli's principle applies to yield that the upper and lower surface speeds must be the same; i.e., $V_u|_{TE} = V_l|_{TE}$. But, for the cusped TE, the Kutta condition implies that $\underline{V}_u|_{TE}$ and $\underline{V}_l|_{TE}$ are in the same direction. This, along with the Bernoulli's principle result, leads to the conclusion that $\underline{V}_u|_{TE} = \underline{V}_l|_{TE}$ in case of a cusped TE.

In conclusion, the mathematical implication of the Kutta condition is

$$\textbf{Kutta condition:} \quad \begin{cases} \text{Wedge TE:} & V_u = V_l = 0 & \text{at TE,} \\ \text{Cusped TE:} & \underline{V}_u = \underline{V}_l & \text{at TE.} \end{cases} \tag{1}$$

It is cautioned that the latter condition only applies in case of incompressible flows; the Kutta condition is anyway only useful in irrotational flows.

3 Two-dimensional source and vortex sheets

We will use two-dimensional source and vortex sheets to model the two-dimensional flow around airfoils. A 2D sheet (e.g., source or vortex sheet) is an extension of a 1D line

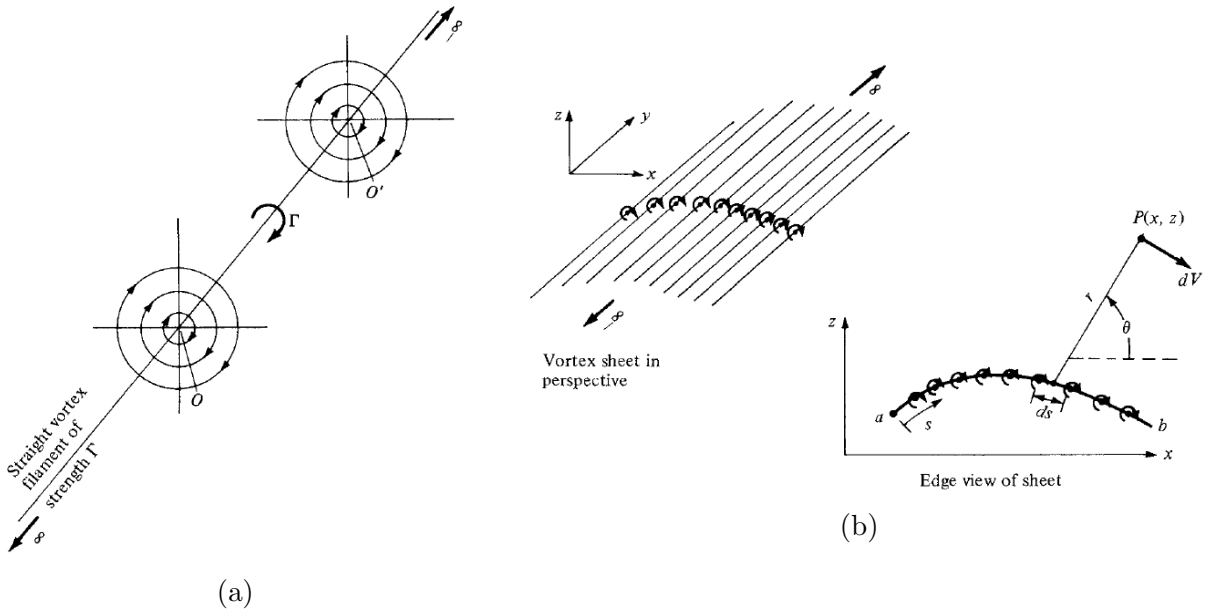

Figure 5: Irrotational vortex singularities: (a) line vortex, and (b) vortex sheet. Adapted from Anderson, Jr., J. D., *Fundamentals of Aerodynamics*, McGraw-Hill, 2011.

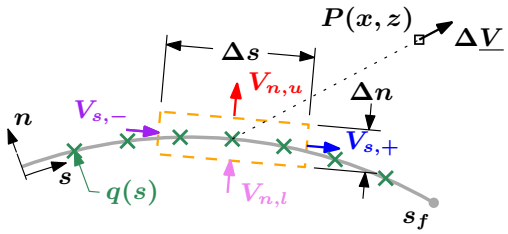

Figure 6: The velocity field associated with a source sheet of source density $q(s)$.

singularity (e.g., line source or line vortex). One can think of a 2D sheet singularity as a one-dimensional array of the corresponding line singularities in a direction perpendicular to the line. For example, figure 5 shows how a 2D vortex sheet can be thought to be constituted from infinitely many discrete line vortices, each of infinitesimal strength. Note that the sheet continues to have infinite extent in the direction in which the constituent line singularity has infinite extent (the $y-$direction in figure 5), and is finite (and possibly curved) in the other direction. We define the local s coordinate to be along the curved sheet, and the n coordinate to be locally normal to the sheet, such that, together with the $y-$coordinate, they form a right-handed curvilinear coordinate system.

3.1 Source sheet

Consider a possibly-curved source sheet as shown in figure 6. The *source density* of the sheet $q(s)$ is defined as the volume flow rate generated by the sheet per unit length (along the s coordinate direction) and per unit span (along the y coordinate direction); it typically varies along the length of the sheet, and is thus a function of s.

We now derive an expression for the near-sheet velocity field. For this, consider the 2D rectangular control volume shown in figure 6, centered around the sheet-aligned coordinate value s. Its length is aligned with the local tangent to the sheet. The velocities just 'above' and 'below' the sheet are denoted by subscripts 'u' and 'l', respectively. Per the definition of the local source density, the net volume flow rate generated by the sheet enclosed within the control volume is $q(s)\Delta s$. In the absence of any other source within this control volume, this must equal the net outflow rate from the four parts of the control surface (recall that the flow is incompressible). We denote the sheet-normal and sheet-tangential velocity components by V_n and V_s, respectively. Thus, we have

$$q(s)\Delta s = \{V_{n,u}(s) - V_{n,l}(s)\}\,\Delta s + \{V_s(s + \Delta s/2) - V_s(s - \Delta s/2)\}\,\Delta n.$$

To focus attention on the extremely near-sheet field, we take the limit as the control volume thickness Δn tends to 0. This leads to the simple conclusion

$$\text{For a general (curved) source sheet:} \qquad V_{n,u}(s) - V_{n,l}(s) = q(s). \tag{2}$$

That is, the effect of a source sheet is to create a *difference* in the local sheet-normal velocity immediately above and below it, the difference being precisely equal to the local source density of the sheet. (Note that, per our choice of the sheet-normal direction $\underline{n}$, $V_{n,u}$ is the sheet-outward velocity above it, and $-V_{n,l}$ is the sheet-outward velocity below it.) The actual magnitudes of these velocities are of course determined by the entire flow field, including all sources and vortices as well as the uniform flow, if any. The reader is urged to check the dimensional consistency of the above equation.

We now determine the velocity at *any* point in the flow domain associated with an infinitesimal length Δs of the source sheet centered at the sheet-aligned coordinate value s, as shown in figure 6. The volume flow rate per unit span generated by this element of the sheet is $q(s)\Delta s$, and it will result in a cylindrically symmetric flow centered on itself. This infinitesimal element of the sheet is essentially a line source, recalling the results for which allows us write down the associated infinitesimal velocity at the arbitrary point $P(x, z)$ as

$$\Delta\underline{V}(x, z) = \frac{q(s)\Delta s}{2\pi}\frac{(x - x(s))\hat{\underline{i}} + (z - z(s))\hat{\underline{k}}}{(x - x(s))^2 + (z - z(s))^2}.$$

Here, $(x(s), z(s))$ is the Cartesian coordinates corresponding to the sheet-aligned coordinate s. The velocity magnitude is inversely proportional to the radial distance from the element to the point P, and the direction is along the outward radius. This expression of course becomes singular at the sheet; we should use the preceding analysis to obtain the near-sheet velocity field.

Finally, the net velocity associated with the entire sheet (extending from $s = 0$ to $s = s_f$, say) is obtained by integration (*vector* addition of infinitesimal contributions)

$$\underline{V}(x, z) = \int_0^{s_f} \frac{q(s)}{2\pi}\frac{(x - x(s))\hat{\underline{i}} + (z - z(s))\hat{\underline{k}}}{(x - x(s))^2 + (z - z(s))^2} ds. \tag{3}$$

It is to be emphasized that this velocity is solely due to the source sheet, and does not account for any other causes (e.g., other sources, vortices or uniform streams).

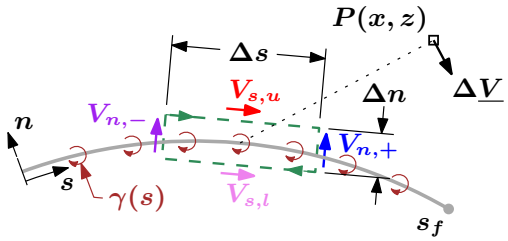

Figure 7: The velocity field associated with a vortex sheet of circulation density $\gamma(s)$.

3.2 Vortex sheet

Consider a possibly-curved vortex sheet as shown in figure 7. The *circulation density* of the sheet $\gamma(s)$ is defined as the circulation around a closed curve enclosing unit length of the sheet (along the s coordinate direction). Note that in aerodynamics convention, the circulation is considered positive if it is clockwise.

We now derive an expression for the near-sheet velocity field in a manner analogous to the preceding developments for a source sheet. For this, consider the planar rectangular closed curve shown in figure 7, centered around the sheet-aligned coordinate value s. Its length is aligned with the local tangent to the sheet. Per the definition of the local circulation density of the sheet, the circulation due to the enclosed sheet element is $\gamma(s)\Delta s$. But, apart from the sheet there is no other vorticity enclosed by the rectangular curve. Thus, the circulation around the closed rectangular curve traversed in the clockwise direction must equal the above circulation generated by the sheet. That is,

$$\gamma(s)\Delta s = \{V_{s,u}(s) - V_{s,l}(s)\}\,\Delta s + \{V_n(s - \Delta s/2) - V_n(s + \Delta s/2)\}\,\Delta n.$$

To focus attention on the extremely near-sheet field, we again take the limit as the control volume thickness Δn tends to 0. This leads to the simple conclusion

$$\text{For a general (curved) vortex sheet:} \qquad V_{s,u}(s) - V_{s,l}(s) = \gamma(s). \tag{4}$$

That is, the effect of a vortex sheet is to create a difference in the local sheet-tangential velocity immediately 'above' and 'below' it, the difference being precisely equal to the local circulation density of the sheet. The actual magnitudes of these velocities are again determined by the entire flow field.

We now determine the velocity at *any* point in the flow domain associated with an infinitesimal length Δs of the vortex sheet centered at the sheet-aligned coordinate value s, as shown in figure 7. The circulation generated by this element of the sheet is $\gamma(s)\Delta s$, and it will result in a cylindrically symmetric flow centered on itself. This infinitesimal element of the sheet is essentially a line irrotational vortex, recalling the results for which allows us write down the associated infinitesimal velocity at the arbitrary point $P(x, z)$ as

$$\Delta\underline{V}(x, z) = \frac{\gamma(s)\Delta s}{2\pi}\,\frac{(z - z(s))\hat{\underline{\imath}} - (x - x(s))\hat{\underline{k}}}{(x - x(s))^2 + (z - z(s))^2}.$$

The magnitude can readily be verified to be inversely proportional to the radial distance from the element to the point P, and it is directed along the clockwise tangent.

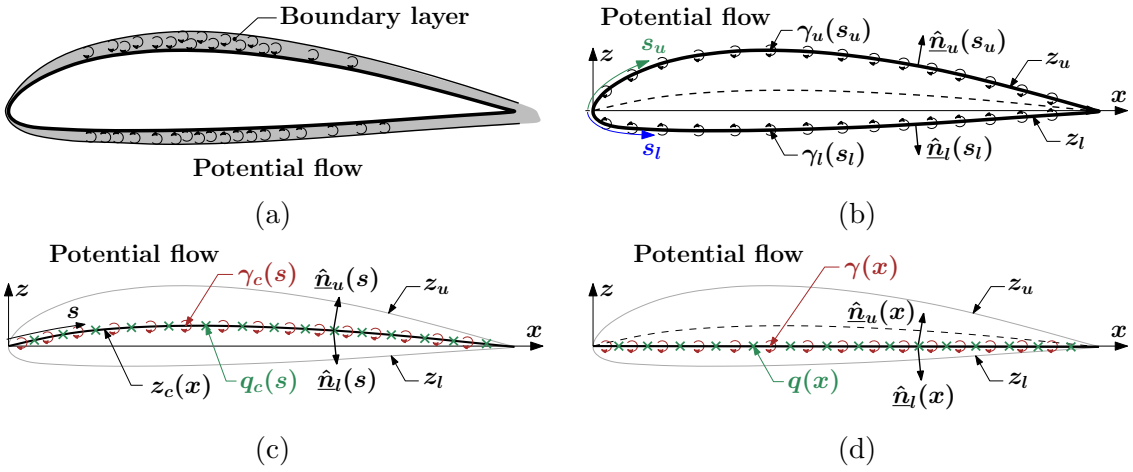

Figure 8: (a) Vorticity concentrated in thin boundary layer; potential flow everywhere else. (b) Vorticity concentrated in a sheet on the airfoil surface; potential flow everywhere outside. (c) Vorticity and source/sink concentrated in a sheet on the airfoil camber line; potential flow everywhere. (d) Vorticity and source/sink concentrated in a sheet on the airfoil chord line; potential flow everywhere.

The net velocity associated with the entire sheet is obtained by integration as in the case of the source sheet:

$$\underline{V}(x,z) = \int_0^{s_f} \frac{\gamma(s)}{2\pi} \frac{(z-z(s))\hat{\underline{i}} - (x-x(s))\hat{\underline{k}}}{(x-x(s))^2 + (z-z(s))^2} ds. \tag{5}$$

4 Hierarchy of Models

The lift on an airfoil can be most accurately calculated by solving the Navier-Stokes equations. In the following, we move through a hierarchy of models, each of which is simpler (and hence more approximate) than the previous. The gain in conceptual insight is intended to make up for the sacrifice of accuracy in this approximation process.

4.1 Boundary layer model

In Prandtl's classic development of the boundary layer model, it was envisaged that the rotational flow is limited to a thin layer wrapping around the airfoil, such that the remainder of the flow is irrotational or potential (see figure 8a). The vorticity distributed within the boundary layer provides the sole contribution to the circulation around the airfoil, which in turn was linked to the lift by Kutta and Joukowsky. Note that the rotational flow also extends into a narrow wake behind the airfoil.

The boundary layer is thin if the Reynolds number is high and the flow is attached, whence the demarcation of the flow into the boundary layer and surrounding irrotational (i.e., potential) outer flow leads to a simpler model.

Considering the boundary conditions, we have no-slip and no-penetration conditions on the surface of the airfoil. In the far field, the flow should relax to the freestream. At the

outer edge of the boundary layer, the pressure is matched with that in the potential flow outside. For the potential flow, the displacement thickness of the boundary layer serves as a modified wall with no penetration.

4.2 Surface vortex sheet model

If the boundary layer is very thin, then a useful approximation is to replace the vorticity distributed across the boundary layer by a concentrated vorticity on the surface of the airfoil, with potential flow assumed everywhere outside the surface – the so-called 'vortex sheet' (see figure 8b); this concept was introduced in § 3.2. In this model, the vortex sheet on the upper and lower surfaces (defined by functions $z_u(x)$ and $z_l(x)$) have respective circulation densities $\gamma_u(s_u)$ and $\gamma_l(s_l)$. A discretized version of this model is solved in the powerful vortex panel method; it will be discussed at length subsequently.

In the absence of viscous effects in our model, the appropriate boundary condition is no-penetration constraint on the surface. That is, the velocity on the upper and lower surfaces should have no components along the respective local normals ($\underline{\hat{n}}_u$ and $\underline{\hat{n}}_l$). To make the solution unique, the Kutta condition has to be specified additionally, as described in § 2. The far-field boundary condition is as before, viz. the flow should revert to the freestream far enough away from the airfoil.

As an aside, we note that while a vortex sheet on the surface of the airfoil is one model, an alternative may be found where the surface is a source sheet (discussed in § 3.1) along with a simpler vortex sheet (possibly of constant circulation density). A discussion of these, and other options, is best left for later when we develop panel methods. However, we note that this points to the essential non-uniqueness of the potential flow models for the outer flow around airfoils.

4.3 Vortex and source sheet on camber line

If the airfoil is thin enough, then the physical separation between its upper and lower surfaces is insignificant. In this case, a useful approximation is to merge the upper and lower surface vortex sheets into a single equivalent vortex sheet (of circulation density γ_c, say) on the camber line running midway between them (see figure 8c). To additionally account for the displacement of the streamlines owing to the thickness of the airfoil (however meagre), one can add a source sheet on the camber line with source density q_c.

The Kutta condition and the far field perturbation decay condition carry over from the previous model. However, the surfaces of the airfoil are no longer modelled explicitly. So, the flow tangency condition is imposed on the upper and lower faces of the camber line, but the unit normals used for this purpose carry over from the corresponding points on the upper and lower surfaces. In other words, for a particular $x-$coordinate along the chord line, we find $\underline{\hat{n}}_u(x)$ (or $\underline{\hat{n}}_l(x)$) from $z_u(x)$ (resp. $z_l(x)$), and then require that the flow velocity just above (resp. below) the camber line (i.e., $z_c(x)$) be normal to this vector.

Although this model is an approximation in the correct direction, it does not yield an analytically tractable solution. Thus it is never used in practice, but serves as a useful conceptual stepping stone to the next model discussed below.

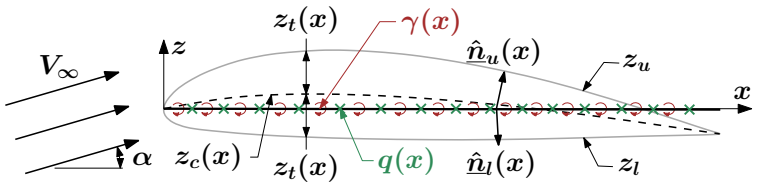

Figure 9: Setup of thin airfoil problem.

4.4 Vortex and source sheet on chord line

If the airfoil does not have a large camber, then the deviation of the camber line from the chord line is insignificant. In this case, a very useful approximation is to flatten the vortex and source sheets from the camber line on to the chord line (see figure 8d). The circulation density of this flat vortex sheet is denoted $\gamma(x)$, and the source density of the flat source sheet is denoted $q(x)$.

The Kutta condition and far field boundary condition carry over from the previous two models. Moreover, the flow tangency condition is applied on the chord line (i.e., $z = 0$), but the unit normals used for this purpose are evaluated from the corresponding points of the upper and lower surface (analogous to the previous model). That is, for a particular $x-$coordinate along the chord line, we find $\underline{\hat{n}}_u(x)$ (or $\underline{\hat{n}}_l(x)$) from $z_u(x)$ (resp. $z_l(x)$), and then require that the flow velocity just above (resp. below) the chord line be normal to this vector.

This model, as it turns out, is very powerful; it yields analytical closed-form results that deliver important insight into aerodynamics as we will see soon. The boundary conditions are used to solve for the circulation density of the vortex sheet and the source density of the source sheet. These singularity distributions are subsequently used to predict the pressure coefficient along the chord (separately on the upper and lower surfaces) using Bernoulli's equation. Integration of this yields the desired lift and pitching moment coefficients of the airfoil section.

5 Setup of thin airfoil problem

The setup of the thin airfoil theory is shown in figure 9. The origin of the coordinate system is placed at the leading edge of the airfoil. To make the setting more general (and hence flexible), we do not constrain the chord of the airfoil to be aligned with the $x-$axis. In particular, the trailing edge of the airfoil need not be on the $x-$axis. The freestream (of speed V_∞) makes the necessary angle of attack α with the $x-$axis.

Of course, there is a non-uniqueness to this setup since any rotation of the coordinate system is valid. However, it will be shown later that this is not an issue in the context of thin airfoil theory. Indeed, the flexibility of the setup will be useful later for simulating airfoils with deflected flaps, say. Note that this setup requires a suitable redefinition of the camber and thickness functions. In particular, unlike earlier, $z_c(x = c) \neq 0$; also, the thickness is defined normal to the $x-$axis, and not to the chord line. Finally, the upper and lower surface functions $z_u(x)$ and $z_l(x)$ have to be redefined too. The actual difference in geometry that results from these modifications are negligible under the prevailing assumptions of thin airfoil

theory. In typical usage, the $x-$axis will be aligned with the chord; only in rare applications (like in the case of the flap deflection problems) will an alternate specification be invoked.

The thin airfoil flow will be simulated using the basic building blocks of potential flow theory, viz. uniform flow, source sheet (instead of line source) and vortex sheet (instead of line irrotational vortex). The source and vortex sheets will be placed along the $x-$axis, as discussed in § 4.4. Since the perturbation due to the airfoil is modelled by the vortex and source sheet, we will denote the (perturbation) velocity due to these two as $u'\hat{\underline{i}} + w'\hat{\underline{k}}$. With an abuse of notation, u and w will respectively denote u' and w' in this note. Being thin, the airfoil is expected to perturb the freestream by a very small amount, so that $|u| \ll V_\infty$ and $|w| \ll V_\infty$. The overall velocity field is

$$\underline{V} = (V_\infty \cos\alpha + u)\hat{\underline{i}} + (V_\infty \sin\alpha + w)\hat{\underline{k}} \approx (V_\infty + u)\hat{\underline{i}} + (V_\infty \alpha + w)\hat{\underline{k}}. \tag{6}$$

The latter simplification follows from the assumed smallness of the angle of attack.

5.1 Boundary conditions

To determine the unique strengths of each of the ingredients - viz. uniform flow, vortex sheet and source sheet, we must satisfy the applicable boundary conditions as discussed herein.

5.1.1 Perturbation decay in the far field

The flow should relax to the freestream far enough away from the airfoil. We use a uniform flow of magnitude and direction equal to that of the freestream. We also note from the analysis presented in Appendix A that the velocity associated with a finite length of a source and/or vortex sheet indeed decays inversely with distance from the sheet. Thus, if the latter are used to model the presence of the airfoil, then the far-field decay of their associated disturbance is guaranteed *a priori*.

5.1.2 Kutta condition

The Kutta condition has been developed in § 2, where it was shown that the flow leaves the trailing edge smoothly if $\underline{V}_u = \underline{V}_l$ thereat. In the thin airfoil problem, the velocity field is a superposition of the effects of the uniform flow and the source and vortex sheets on the chord line. Thus, using the expression for this velocity field from eqn (6), the Kutta condition is specialized to

$$u(c, 0^+) = u(c, 0^-) \quad \text{and} \quad w(c, 0^+) = w(c, 0^-).$$

It is shown in § 3.1 that only a source sheet can be associated with a difference in *local* sheet-normal velocity above and below itself. Thus, the $w(c, 0^+) = w(c, 0^-)$ condition implies that $q(c) = 0$. However, this is not remarkable, as this same criterion could also be reached from the very fact that the trailing edge is sharp (so that there is no normal displacement of the flow thereat).

The more important condition is the first one, viz. $u(c, 0^+) = u(c, 0^-)$. Recalling from § 3.2 that only a vortex sheet can cause a differential *local* sheet-tangential velocity, we

readily conclude that

$$\text{Kutta condition for thin airfoil theory:} \qquad \gamma(c)\,(\equiv \gamma(TE)) = 0. \tag{7}$$

That the Kutta condition imposes a constraint on the vortex sheet alone is not surprising, given the fact that it is only the circulation around the airfoil (which is the total circulation of the vortex sheet) that is uniquely determined by this condition.

Note that the above mathematical expression of the Kutta condition is not restricted to planar vortex sheets (as considered in the thin airfoil theory); it is equally valid for an isolated curved vortex sheet (as may be distributed on the camber line – see § 4.3). This is because the results used above were derived for general source and vortex sheets. However, strictly speaking, it is not applicable to the surface vortex sheet model of § 4.2 for a wedge-shaped trailing edge, since in that case there are *two* vortex sheets – one on the upper and another on the lower surface – that meet at the trailing edge.

5.1.3 No-penetration condition

In the context of thin airfoil theory, the no-penetration condition is specified as

$$\underline{V}(x, 0^+) \cdot \hat{\underline{n}}_u(x) = 0, \qquad \text{and} \qquad \underline{V}(x, 0^-) \cdot \hat{\underline{n}}_l(x) = 0, \qquad x \in (0, c). \tag{8}$$

Note that, per the preceding setup, this condition is applied on the velocity evaluated on the chord line, and not on the actual surfaces.

To apply the above boundary condition, we will now develop an expression for the surface normal with the help of figure 10. Consider the generic surface specified by $z_s(x)$; in other words, the equation of the surface is $z - z_s(x) = 0$. There are several approaches to finding the local surface normal.

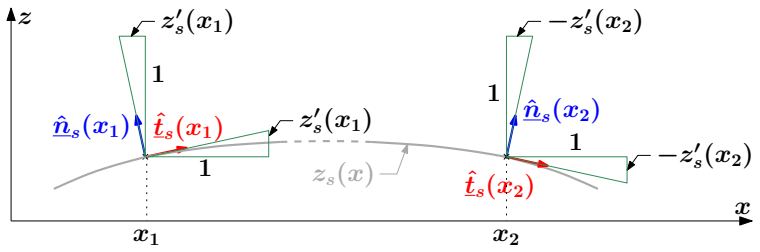

Figure 10: Geometry of surface normal and tangent for two-dimensional surfaces.

In the first approach, we appeal directly to geometry (an alternative is described in Appendix B). We note from figure 10 that the local surface tangent is in the direction $[\hat{\underline{i}} + z_s'(x)\hat{\underline{k}}]$. Here, z_s' is the derivative of z_s with respect to its argument (x in this case). Note that this expression is valid at both $x = x_1$ where the slope is positive, and at $x = x_2$ where it is negative. From the geometry, we conclude that the direction of the local surface normal is $-z_s'(x)\hat{\underline{i}} + \hat{\underline{k}}$, irrespective of the actual sign of the slope.

The magnitudes of both the tangent and normal vectors found above are $\sqrt{1 + (z_s')^2}$. Given that the airfoil is thin and lightly cambered, the surface slope is small everywhere, so

that the above magnitude is close to unity. Thus, the preceding tangent and normal vectors are also approximately *unit* vectors. In summary, we have

$$\text{Unit normal to surface } z_s(x): \qquad \underline{\hat{n}}_s(x) \approx -z_s'(x)\underline{\hat{i}} + \underline{\hat{k}}, \tag{9}$$

$$\text{Unit tangent to surface } z_s(x): \qquad \underline{\hat{t}}_s(x) \approx \underline{\hat{i}} + z_s'(x)\underline{\hat{k}}. \tag{10}$$

Note that the expression for the surface normal is agnostic to the 'outward' or 'inward' nature of the normal. This is not an issue here as we are only interested in *not* having any flow along the surface normal, be it inward or outward. The tangent direction found above is along the general direction of $+x$, which will be recalled to be the general direction of positive freestream (modulo the angle-of-attack correction).

The unit normals on the upper and lower surfaces of the thin airfoil are

$$\text{Unit normal on upper surface } z_u(x): \qquad \underline{\hat{n}}_u(x) = -(z_c'(x) + z_t'(x))\underline{\hat{i}} + \underline{\hat{k}},$$

$$\text{Unit normal on lower surface } z_l(x): \qquad \underline{\hat{n}}_l(x) = -(z_c'(x) - z_t'(x))\underline{\hat{i}} + \underline{\hat{k}}.$$

Using the expressions for velocity field and surface normals developed above, we compactly write the boundary conditions for the upper and lower surfaces (see eqn (8)) as

$$\begin{aligned} &\left[\left\{V_\infty + u(x,0^\pm)\right\}\underline{\hat{i}} + \left\{V_\infty\alpha + w(x,0^\pm)\right\}\underline{\hat{k}}\right] \cdot \left[-\left\{z_c'(x) \pm z_t'(x)\right\}\underline{\hat{i}} + \underline{\hat{k}}\right] = 0, \quad x \in (0,c) \\ \implies &-\left\{V_\infty + u(x,0^\pm)\right\}\left\{z_c'(x) \pm z_t'(x)\right\} + V_\infty\alpha + w(x,0^\pm) = 0, \quad x \in (0,c). \end{aligned}$$

In the $\pm$ symbol, the $+$ sign applies to the upper surface and the $-$ sign applies to the lower surface of the chord line. We now recall that the perturbation speed u is assumed to be much smaller than the freestream speed V_∞. Thus, we arrive at the following constraint on the $z-$component of the perturbation velocity in the thin airfoil problem

$$\frac{w(x,0^\pm)}{V_\infty} = -\alpha + z_c'(x) \pm z_t'(x), \qquad x \in (0,c). \tag{11}$$

This is variously called the 'airfoil equation' or 'aerofoil equation'.

Discussion: Owing to the series of careful approximations made till this point, we have arrived at a very elegant problem. The three geometry parameters of the thin airfoil problem appear separately in the above constraint equation, viz. the angle of attack, the thickness of the airfoil, and its camber. Since the potential flow theory is linear and the above boundary condition is also linear, we can readily divide the thin airfoil problem into three sub-problems:

AoA problem: Find vortex sheet $\gamma(x)$ s.t. $\dfrac{w(x,0^\pm)}{V_\infty} = -\alpha, \quad x \in (0,c),$ (12)

Camber problem: Find vortex sheet $\gamma(x)$ s.t. $\dfrac{w(x,0^\pm)}{V_\infty} = z_c'(x), \quad x \in (0,c),$ (13)

Thickness problem: Find source sheet $q(x)$ s.t. $\dfrac{w(x,0^\pm)}{V_\infty} = \pm z_t'(x), \quad x \in (0,c).$ (14)

Note that we have also separated the reasons for having the vortex and source sheet. In particular, the plane source sheet is only required to simulate the thickness effect of the airfoil. As discussed in Appendix A it exclusively creates the equal and opposite sheet-normal velocities above and below itself, as mandated by the thickness problem. On the other hand, the angle-of-attack and camber problems require the same sheet-normal velocities above and below the chord line, and hence cannot involve a plane source sheet; these problems thus involve the plane vortex sheet exclusively. This demarcation also agrees with experimental observations that relate lift (and hence, circulation and vorticity) to the angle-of-attack and camber, and not to the thickness of the airfoil (for thin airfoils).

6 Pressure coefficient in thin airfoil theory

Before we actually solve the thin airfoil problem, we derive an approximate expression for the surface pressure coefficient on the airfoil that is consistent with the prevailing assumptions. For the irrotational, incompressible, steady, inviscid flow used to model the airfoil, Bernoulli's equation is applicable between any two points. In particular, we apply it between a point in the freestream and the point of interest. Then, the pressure coefficient is

$$\begin{aligned} c_p = \frac{p - p_\infty}{0.5\rho_\infty V_\infty^2} &= \frac{0.5\rho_\infty V_\infty^2 - 0.5\rho_\infty V^2}{0.5\rho_\infty V_\infty^2} = 1 - \frac{(V_\infty \cos\alpha + u)^2 + (V_\infty \sin\alpha + w)^2}{V_\infty^2} \\ &= 1 - \frac{V_\infty^2 + 2V_\infty u\cos\alpha + u^2 + w^2 + 2V_\infty w \sin\alpha}{V_\infty^2}. \end{aligned}$$

It will be recalled that, in the thin airfoil problem, $|u| \ll V_\infty$, $|w| \ll V_\infty$ and α is very small. Thus, the above expression simplifies to

$$\text{Pressure coefficient in thin airfoil theory:} \qquad c_p \approx -\frac{2u}{V_\infty}. \tag{15}$$

7 Solution of the angle-of-attack problem

The angle-of-attack problem statement is (see figure 11): given a freestream of speed V_∞ making an angle α with a flat plate, find the necessary circulation density distribution $\gamma(x)$ of the vortex sheet on the chord line ($z = 0$) such that

$$w(x, 0^\pm) = -V_\infty \alpha, \qquad x \in (0, c),$$

subject to the Kutta condition. In essence, we require that the sheet-normal velocity associated with the vortex sheet to equal and oppose the sheet-normal component of the freestream at every point on the chord. This is true both above and below the sheet. The vortex sheet cannot generate any differential sheet-normal velocity across it, and none is required by the above constraint.

The (perturbation) velocity due to a planar vortex sheet can be found from the results presented in Appendix A.2. In particular, the $z-$component of velocity just above and below

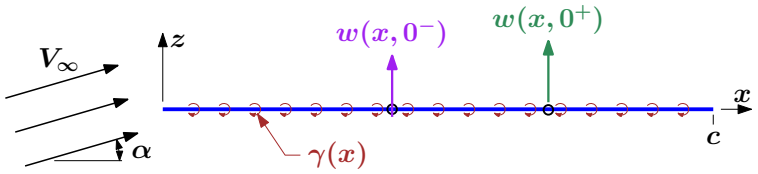

Figure 11: Setup of the angle-of-attack problem of thin airfoil theory.

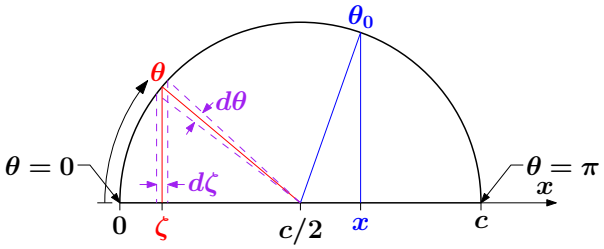

Figure 12: Coordinate transformation in aerodynamics.

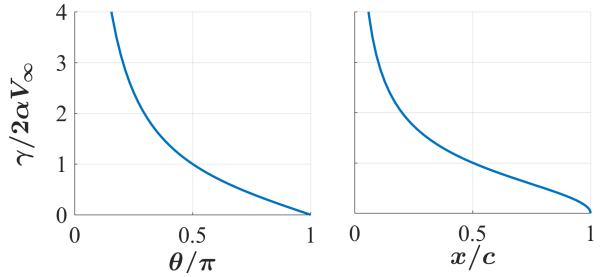

Figure 13: Vortex sheet circulation density function for angle-of-attack problem.

the sheet are expressed in terms of the integrated circulation density as

$$w_u(x) = w_l(x) = -\frac{1}{2\pi}\int_0^c \frac{\gamma(\zeta)}{x-\zeta}d\zeta.$$

This is used in the above constraint equation to arrive at the following *integral equation* for γ (subject to the Kutta condition):

$$\frac{1}{2\pi}\int_0^c \frac{\gamma(\zeta)}{x-\zeta}d\zeta = V_\infty\alpha, \qquad x \in (0,c), \tag{16a}$$

$$\gamma(c) = 0. \tag{16b}$$

This problem was formulated and elegantly solved by Glauert. We will follow along in his steps to understand the procedure.

Coordinate transformation: Glauert first introduced the following ingenious change of variable

$$x = \frac{c}{2}(1-\cos\theta_0), \qquad \zeta = \frac{c}{2}(1-\cos\theta), \qquad d\zeta = \frac{c}{2}\sin\theta\, d\theta, \qquad x \in (0,c), \quad \theta \in (0,\pi).$$

As shown in figure 12, θ runs from 0 at the leading edge to π at the trailing edge. As the transformation is invertible, functions of ζ (or x) can be expressed in terms of θ (resp. θ_0).

The constraint equations on the circulation density distribution now become

$$\frac{1}{2\pi}\int_0^\pi \frac{\gamma(\theta)\sin\theta}{\cos\theta-\cos\theta_0}d\theta = V_\infty\alpha, \qquad \theta_0 \in (0,\pi), \tag{17a}$$

$$\gamma(\pi) = 0. \tag{17b}$$

Even this integral equation is not trivial to solve. However, we invoke (without proof) two standard definite integrals in aerodynamics (found by Glauert again)

$$\int_0^\pi \frac{\cos n\theta}{\cos\theta - \cos\theta_0} d\theta = \frac{\pi \sin n\theta_0}{\sin\theta_0}, \tag{18a}$$

$$\int_0^\pi \frac{\sin n\theta \sin\theta}{\cos\theta - \cos\theta_0} d\theta = -\pi \cos n\theta_0, \tag{18b}$$

where n is an integer, and use these to claim (see plot in figure 13)

$$\boxed{\text{AoA problem solution:} \quad \gamma(\theta) = 2V_\infty \alpha \frac{1+\cos\theta}{\sin\theta} = 2V_\infty \alpha \cot\frac{\theta}{2}, \quad \theta \in (0,\pi).} \tag{19}$$

To verify, we substitute this in eqn (17a) and use eqn (18a):

$$\begin{aligned}\frac{V_\infty \alpha}{\pi} \int_0^\pi \frac{1+\cos\theta}{\cos\theta - \cos\theta_0} d\theta &= \frac{V_\infty \alpha}{\pi} \int_0^\pi \frac{\cos(0\times\theta) + \cos(1\times\theta)}{\cos\theta - \cos\theta_0} d\theta \\ &= \frac{V_\infty \alpha}{\pi} \frac{\pi}{\sin\theta_0} \left[\sin(0\times\theta_0) + \sin(1\times\theta_0)\right] = V_\infty \alpha. \qquad \text{Q.E.D.}\end{aligned}$$

The Kutta condition is easily verified as $\cot \pi/2 = 0$ indeed.
In terms of the original ζ coordinates, we have the solution:

$$\frac{\gamma(\zeta)}{2V_\infty \alpha} = \frac{1+\cos\theta}{\sin\theta} = \frac{1+\cos\theta}{\sqrt{1-\cos^2\theta}} = \sqrt{\frac{1+\cos\theta}{1-\cos\theta}} = \sqrt{\frac{1+(1-2\zeta/c)}{2\zeta/c}} = \sqrt{\frac{c-\zeta}{\zeta}}.$$

Since there is no ambiguity, we express this in terms of x (as plotted in figure 13 also)

$$\gamma(x) = 2V_\infty \alpha \sqrt{\frac{c-x}{x}}, \qquad x \in (0,c). \tag{20}$$

It will be noted from figure 13 that the circulation density tends to infinity at the leading edge. This is of course not physical, but the model attempts to simulate the condition of the stagnation point being on the pressure surface of the flat plate, and the flow having to thus curl around the sharp leading edge. This singularity is however weak (integrable), in the sense that the integrated results for c_l and c_m are still valid.

Plate-surface velocity: It will be recalled from Appendix A.2 that a plane vortex sheet creates equal and opposite sheet-tangential velocity perturbations (u) locally above and below itself, both being equal in magnitude to half the local circulation density; i.e., $u_u(x) = -u_l(x) = \gamma(x)/2$. Using eqn (20), we have

$$u_u(x) = \frac{\gamma(x)}{2} = V_\infty \alpha \sqrt{\frac{c-x}{x}}, \qquad u_l(x) = -\frac{\gamma(x)}{2} = -V_\infty \alpha \sqrt{\frac{c-x}{x}}, \qquad x \in (0,c). \tag{21}$$

This is presented in normalized fashion in figure 14a. Of course, the overall velocity in the $x-$direction is approximately $V_\infty + u$.

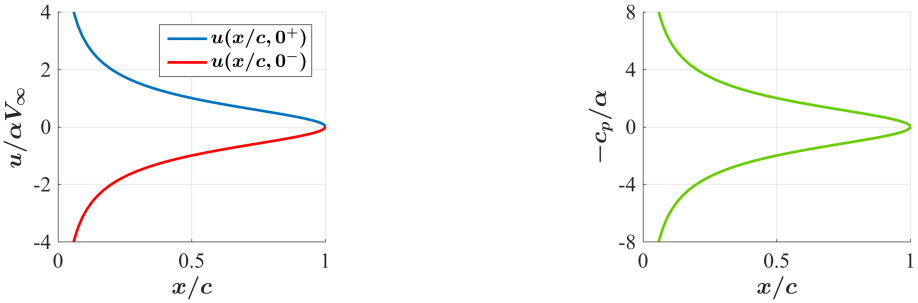

(a) (b)

Figure 14: (a) Normalized plate-tangential surface velocity perturbation, and (b) normalized pressure coefficient, in angle-of-attack problem solution.

Plate surface pressure coefficient: The preceding result, along with eqn (15) (i.e., $c_p = -2u/V_\infty$), can be used to approximate the pressure coefficient above and below the flat plate:

$$c_{p,u}(x) = -\frac{\gamma(x)}{V_\infty} = -2\alpha\sqrt{\frac{c-x}{x}}, \qquad c_{p,l}(x) = \frac{\gamma(x)}{V_\infty} = 2\alpha\sqrt{\frac{c-x}{x}}, \qquad x \in (0, c). \tag{22}$$

This behaviour is plotted in figure 14b. Indeed, thin airfoil theory predicts suction on the upper surface and equal pressure on the lower one, the distribution being symmetric about the plate. Recall that the area enclosed by the c_p plot is the sectional lift coefficient c_l. Thus, we get an early indication that $c_l \propto \alpha$ for a flat plate per thin airfoil theory. We will quantify this proportionality next.

Lift coefficient: We can find c_l (and hence c_m) in two equivalent ways: (a) calculate the surface pressure coefficient and integrate that, or (b) integrate the circulation density to obtain an overall circulation and relate it to lift using Kutta-Joukowsky theorem.

We will take the first route, and lead up to the second one. Using the result from eqn (22), the pressure 'loading' on the flat plate is

$$(p_l - p_u)(x) = \frac{1}{2}\rho_\infty V_\infty^2 \left[c_{p,l}(x) - c_{p,u}(x)\right] = \frac{1}{2}\rho_\infty V_\infty^2 \frac{2\gamma(x)}{V_\infty} = \rho_\infty V_\infty \gamma(x).$$

The infinitesimal sectional lift dL' generated by the infinitesimal element dx at a point x along the plate is $(p_l - p_u)dx$. Thus, the infinitesimal contribution to the sectional lift coefficient from this element of the plate is

$$dc_l = \frac{dL'}{0.5\rho_\infty V_\infty^2 c} = \frac{(p_l - p_u)dx}{0.5\rho_\infty V_\infty^2 c} = (c_{p,l} - c_{p,u})\frac{dx}{c} = 2\frac{\gamma(x)dx}{V_\infty c}.$$

The sectional lift coefficient can now be found by integration:

$$c_l = \int_0^c dc_l = \frac{2}{V_\infty c}\int_0^c \gamma(x)dx =: \frac{2\Gamma}{V_\infty c},$$

where $\Gamma := \int_0^c \gamma(x)dx$ is the total circulation due to the vortex sheet. Unsurprisingly, this agrees with the Kutta-Joukowsky theorem:

$$c_l = \frac{L'}{0.5\rho_\infty V_\infty^2 c} = \frac{\rho_\infty V_\infty \Gamma}{0.5\rho_\infty V_\infty^2 c} = \frac{2\Gamma}{V_\infty c}.$$

The actual calculation of the circulation is most readily conducted in the transformed θ coordinate by direct substitution (writing θ_0 as θ since there is no need for a dummy variable anymore):

$$\begin{aligned}\Gamma &= \int_0^c \gamma(x)dx = \frac{c}{2}\int_0^\pi \gamma(\theta)\sin\theta\ d\theta = \frac{c}{2}\int_0^\pi \left(2V_\infty\alpha\frac{1+\cos\theta}{\sin\theta}\right)\sin\theta\ d\theta \\ &= cV_\infty\alpha\int_0^\pi (1+\cos\theta)d\theta = cV_\infty\alpha\left[\theta+\sin\theta\right]_0^\pi = \pi c V_\infty\alpha.\end{aligned}$$

The lift coefficient is then

$$\boxed{c_l = 2\pi\alpha.} \tag{23}$$

This is a very important result, showing that the lift is proportional to the angle of attack. Since the angle of attack doesn't appear anywhere else in the theory, and the thickness of the airfoil cannot affect lift in the context of thin airfoil theory, the above result applies to *all* thin symmetric airfoils. Figure 15 demonstrates that this theory is astonishingly accurate for high-Reynolds number flow over thin symmetric airfoils, given the many (albeit careful) approximations made along the way.

The predicted *lift slope* is

$$\boxed{\frac{\partial c_l}{\partial\alpha} = 2\pi = 0.11 \text{ per degree.}} \tag{24}$$

Since the angle of attack doesn't appear anywhere else in the thin airfoil theory, this is the predicted lift slope for *all* thin airfoils, even those with camber (albeit small, so as to satisfy the assumptions of thin airfoil theory)! Indeed, we have previously seen experimental data of lightly cambered airfoils displaying the same lift slope as their symmetric counterparts.

Pitching moment coefficient: The sectional pitching moment about the leading edge is found by integrating the contributions of each infinitesimal section of the chord:

$$\begin{aligned}M'_{LE} &= \int_0^c dM'_{LE} = -\int_0^c x\ dL' = -\rho_\infty V_\infty\int_0^c x\gamma(x)dx \\ &= -\rho_\infty V_\infty\int_0^\pi \frac{c(1-\cos\theta)}{2}\left(2V_\infty\alpha\frac{1+\cos\theta}{\sin\theta}\right)\left(\frac{c}{2}\sin\theta\ d\theta\right) = -\frac{1}{2}\rho_\infty V_\infty^2 c^2\alpha\int_0^\pi \sin^2\theta\ d\theta \\ &= -\frac{1}{4}\rho_\infty V_\infty^2 c^2\alpha\int_0^\pi (1-\cos 2\theta)d\theta = -\frac{1}{4}\rho_\infty V_\infty^2 c^2\alpha\left[\theta-\frac{\sin 2\theta}{2}\right]_0^\pi = -\frac{\pi}{4}\rho_\infty V_\infty^2 c^2\alpha.\end{aligned}$$

Thus, the sectional pitching moment coefficient about the leading edge is

$$c_{m,LE} = \frac{-\pi\alpha}{2} = -\frac{c_l}{4}. \tag{25}$$

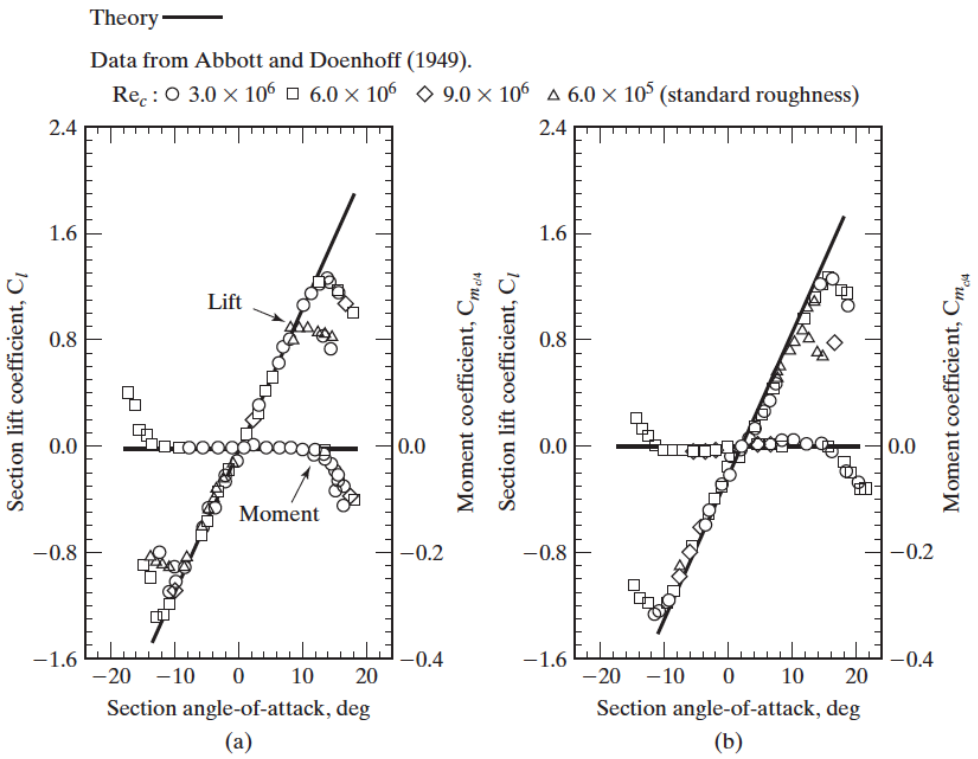

Figure 15: Comparison of the aerodynamic coefficients calculated using thin-airfoil theory against data from Abbott and von Doenhoff (1949) for two symmetric airfoils: (a) NACA 0009, and (b) NACA 0012-64 [adopted from Bertin and Cummings (2013)].

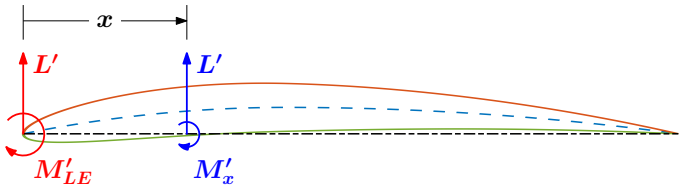

Figure 16: Two equivalent force-moment systems shown in red and blue.

Figure 16 shows two equivalent force-moment systems. We can either calculate the pitching moment about the leading edge, in which case the associate lift force is taken to be acting through the leading edge. Alternatively, the pitching moment can be evaluated about any other point on the chord (say at x), in which case the resultant force (lift, in this case) is taken to act through this point. Evidently, the pitching moments in the two cases are related as

$$M'_x = M'_{LE} + L'x, \qquad c_{m,x} = c_{m,LE} + c_l \frac{x}{c}.$$

It will be recalled that the center of pressure is the point about which the pitching moment vanishes. Reference to the above equation shows that, for the flat plate under consideration, the center of pressure is the quarter-chord point $x = c/4$, and this result is evidently independent of the angle of attack.

It will also be recalled that the aerodynamic center is the point about which the pitching

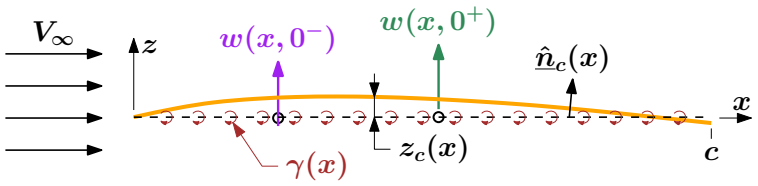

Figure 17: Setup of the camber problem of thin airfoil theory.

moment remains (at least approximately) constant, irrespective of the angle of attack. Since the pitching moment vanishes about the quarter-chord point for all α, this point is also the aerodynamic center. Thus, we have the important conclusion:

$$\boxed{\text{For all symmetric airfoils:} \quad x_{ac} = x_{cp} = \frac{c}{4}, \qquad c_{m,ac} = c_{m,cp} = 0.} \tag{26}$$

Figure 15 demonstrates the validity of this conclusion.

Note that the other (camber and thickness) subproblems are necessarily independent of the angle of attack. Thus,

$$\boxed{\text{For all thin airfoils:} \quad x_{ac} = \frac{c}{4}.} \tag{27}$$

Of course, $c_{m,ac} \neq 0$ for cambered airfoils, as we find next.

8 Solution of the camber problem

The camber problem statement is (see figure 17): given a freestream of speed V_∞ aligned with the chord of a cambered flat pate, find the necessary circulation density distribution $\gamma(x)$ of the vortex sheet on the chord line ($z = 0$) such that

$$w(x, 0^\pm) = V_\infty z_c'(x), \qquad x \in (0, c),$$

subject to the Kutta condition. It is to be remembered that, the trailing edge of the camber line need not lie on the $x-$axis. In essence, we require that the sheet-normal velocity associated with the vortex sheet to equal the camber-normal component of the freestream at every point on the chord. This is true both above and below the sheet. The vortex sheet cannot generate any differential sheet-normal velocity across it, and none is required by the above constraint.

Using the expression for the sheet-normal velocity developed for a plane vortex sheet in Appendix A.2, we arrive at the following *integral equation* for γ:

$$\frac{1}{2\pi} \int_0^c \frac{\gamma(\zeta)}{x - \zeta} d\zeta = -V_\infty z_c'(x), \qquad x \in (0, c),$$

subject to the Kutta condition formulated as

$$\gamma(c) = 0.$$

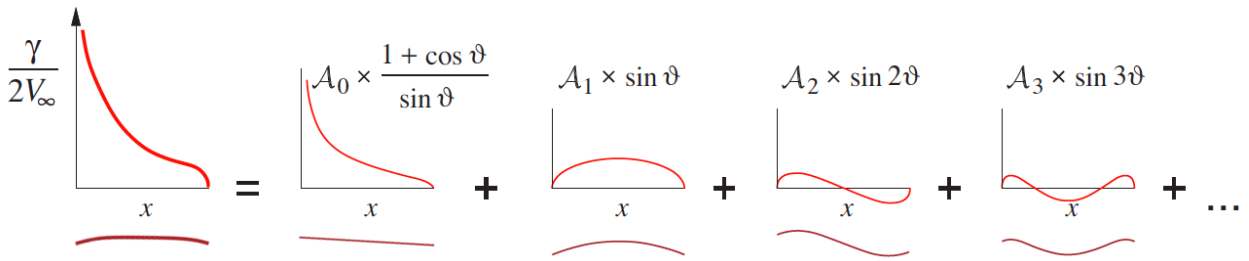

Figure 18: Vortex sheet strength series components. Each component is associated with a specific camberline geometry mode sketched below it. [Adopted from Drela, M., Flight vehicle aerodynamics, MIT Press, 2014.]

Applying the aerodynamic coordinate transformation, the restated problem is

$$\frac{1}{2\pi}\int_0^\pi \frac{\gamma(\theta)\sin\theta}{\cos\theta-\cos\theta_0}d\theta = -V_\infty \frac{dz_c}{dx}(\theta_0), \qquad \theta_0 \in (0,\pi), \tag{28a}$$

$$\gamma(\pi) = 0. \tag{28b}$$

It is made explicit above that dz_c/dx is to be evaluated at angle θ_0; the continued use of the notation $z_c'(\theta_0)$ would have confused the reader that z_c should first be expressed as a function of θ_0, and then differentiated with respect to this argument – this is *not* the case.

The camber derivative function is smooth. Let us write it as

$$\frac{dz_c}{dx}(\theta_0) = \underbrace{\frac{1}{\pi}\int_0^\pi \frac{dz_c}{dx}(\theta)d\theta}_{\text{Average}} + \underbrace{\left[\frac{dz_c}{dx}(\theta_0) - \frac{1}{\pi}\int_0^\pi \frac{dz_c}{dx}(\theta)d\theta\right]}_{\text{Fluctuation}}.$$

Since the problem is linear, the solution $\gamma(\theta)$ can also be separated into a contribution from the (constant) average part of the camber derivative function and another from its (zero-mean) fluctuating part. The solution of the first problem is already known from the angle-of-attack problem, where the right hand side was indeed constant. Recalling this solution, and noting the Kutta condition, the overall solution thus must have the form

$$\gamma(\theta) = 2V_\infty\left(A_0\frac{1+\cos\theta}{\sin\theta} + \sum_{n=1}^{\infty} A_n \sin n\theta\right). \tag{29}$$

We have introduced the constant factor V_∞ to render the coefficients dimensionless; the factor of 2 follows standard convention.

Essentially, we expand the (as yet unknown) solution $\gamma(\theta)$ as the known form contributed by a constant RHS, added to a general Fourier series (with cosine and sine terms); see figure 18. It will be recalled that such a Fourier series expansion is warranted whenever the function is periodic over the circular coordinate θ and is square-integrable. In the present instance, $\gamma(\theta)$ is only required to be defined over $(0,\pi)$, and thus we are at liberty to design it in the remaining half $(-\pi,0)$ so as to have the necessary periodicity. We subsequently realize that all the cosine terms must vanish so that the Kutta condition $\gamma(\pi)=0$ may be

satisfied. Note that the assumption of integrability of γ is not far-fetched; the circulation (and lift) must ultimately be obtained by integrating this function.

Substituting the above assumed form of the solution in the constraint equation eqn (28a) (it already satisfies eqn (28b)), and using the aerodynamic integrals from eqn (18), we have

$$\frac{1}{2\pi}\int_0^\pi \frac{\gamma(\theta)\sin\theta}{\cos\theta-\cos\theta_0}d\theta = \frac{V_\infty}{\pi}\int_0^\pi \left[A_0\frac{1+\cos\theta}{\sin\theta}+\sum_{n=1}^{\infty}A_n\sin n\theta\right]\frac{\sin\theta}{\cos\theta-\cos\theta_0}d\theta$$
$$= V_\infty\left(A_0-\sum_{n=1}^{\infty}A_n\cos n\theta_0\right) = -V_\infty\frac{dz_c}{dx}(\theta_0), \qquad \theta_0\in(0,\pi).$$

As argued earlier, this involves separating the RHS into a constant part and a zero-mean fluctuating part. This also suggests, that the unknown coefficients of the solution A_n are to be found from the cosine transform of the camber derivative function. Note that this is not restrictive since the actual camber derivative function is only defined in the half period $[0,\pi]$. It can therefore be extended without loss of generality as an even function to the remaining half period, so as to satisfy the criterion for a cosine series expansion. (The even function extension allows for a non-zero value at the origin, and is hence a more general extension than an odd function extension.) It will be recalled that the sine terms are absent owing to the Kutta condition.

Recall that the cosine transform of $dz_c/dx(\theta)$ is defined as

$$\frac{dz_c}{dx}(\theta) = B_0+\sum_{m=1}^{\infty}B_m\cos m\theta, \qquad B_0=\frac{1}{\pi}\int_0^\pi\frac{dz_c}{dx}(\theta)d\theta, \quad B_m=\frac{2}{\pi}\int_0^\pi\frac{dz_c}{dx}(\theta)\cos m\theta\ d\theta.$$

Comparing terms, we have the expressions for the coefficients appearing in eqn (29):

$$A_0 = -\frac{1}{\pi}\int_0^\pi\frac{dz_c}{dx}(\theta)d\theta, \qquad A_n=\frac{2}{\pi}\int_0^\pi\frac{dz_c}{dx}(\theta)\cos n\theta\ d\theta. \tag{30}$$

Lift coefficient: With the circulation density solution at hand, the sectional lift coefficient due solely to camber can be readily found by integrating it (as in the AoA problem):

$$c_l = \frac{2}{V_\infty c}\int_0^c\gamma(x)dx = \frac{1}{V_\infty}\int_0^\pi\gamma(\theta)\sin\theta\ d\theta = 2\int_0^\pi\left(A_0\frac{1+\cos\theta}{\sin\theta}+\sum_{n=1}^{\infty}A_n\sin n\theta\right)\sin\theta\ d\theta$$
$$= 2A_0\int_0^\pi(1+\cos\theta)d\theta + 2\sum_{n=1}^{\infty}A_n\int_0^\pi\sin n\theta\ \sin\theta\ d\theta.$$

The first integral has already been found to evaluate to π. The second integral is of the general form

$$\int_0^\pi\sin n\theta\ \sin m\theta\ d\theta = \frac{\pi}{2}\delta_{nm},$$

owing to the orthogonality of the Fourier basis. Recalling eqn (23), we have the final result

$$\boxed{\text{For } \textit{all} \text{ thin airfoils:} \quad c_l = 2\pi\alpha+(2A_0+A_1)\,\pi = 2\pi\alpha+2\int_0^\pi\frac{dz_c}{dx}(\theta)\,(\cos\theta-1)\,d\theta.} \tag{31}$$

Pitching moment coefficient: As in the angle-of-attack problem, we calculate the sectional pitching moment about the leading edge due to the camber alone as

$$\begin{aligned}
M'_{LE} &= -\rho_\infty V_\infty \int_0^c x\gamma(x)dx \\
&= -2\rho_\infty V_\infty^2 \int_0^\pi \frac{c(1-\cos\theta)}{2}\left(A_0\frac{1+\cos\theta}{\sin\theta}+\sum_{n=1}^{\infty}A_n\sin n\theta\right)\left(\frac{c}{2}\sin\theta\ d\theta\right) \\
&= -\frac{1}{2}\rho_\infty V_\infty^2 c^2\left[A_0\int_0^\pi \sin^2\theta\ d\theta+\sum_{n=1}^{\infty}A_n\int_0^\pi(1-\cos\theta)\sin n\theta\sin\theta\ d\theta\right] \\
&= -\frac{1}{2}\rho_\infty V_\infty^2 c^2\left[\frac{A_0}{2}\int_0^\pi(1-\cos 2\theta)d\theta+\sum_{n=1}^{\infty}A_n\int_0^\pi\sin n\theta\left\{\sin\theta-\frac{1}{2}\sin 2\theta\right\}d\theta\right] \\
&= -\frac{\pi}{4}\rho_\infty V_\infty^2 c^2\left[A_0+\sum_{n=1}^{\infty}A_n\left\{\delta_{n1}-\frac{1}{2}\delta_{n2}\right\}\right] = -\frac{\pi}{4}\rho_\infty V_\infty^2 c^2\left(A_0+A_1-\frac{1}{2}A_2\right).
\end{aligned}$$

Thus, the sectional pitching moment coefficient referred to the leading edge is

$$c_{m,LE} = -\frac{\pi}{2}\left(A_0+A_1-\frac{1}{2}A_2\right) = -\frac{1}{2}\int_0^\pi \frac{dz_c}{dx}(\theta)\left(2\cos\theta-\cos 2\theta-1\right)d\theta.$$

The corresponding pitching moment referred to the quarter-chord point is

$$c_{m,c/4} = c_{m,LE}+\frac{c_l}{4} = -\frac{\pi}{4}(A_1-A_2) = -\frac{1}{2}\int_0^\pi \frac{dz_c}{dx}(\theta)\left(\cos\theta-\cos 2\theta\right)d\theta.$$

It will be recalled from the angle-of-attack problem solution that the quarter-chord point is the aerodynamic center for all thin airfoils. Thus,

$$\boxed{\text{For } \textit{all} \text{ thin airfoils:}\quad c_{m,ac} = c_{m,c/4} = -\frac{1}{2}\int_0^\pi \frac{dz_c}{dx}(\theta)\left(\cos\theta-\cos 2\theta\right)d\theta.} \tag{32}$$

8.1 Results

Figure 19 demonstrates that the prediction of lift coefficient from thin airfoil theory is quite accurate, as long as viscous effects (like stalling) are insignificant. However, slight discrepancies are apparent in the case of the thicker airfoil. The quarter-chord moment coefficient, on the other hand, does not appear to be estimated properly. In particular, the quarter-chord does not even appear to be the aerodynamic center. In fact, for these two airfoils, the aerodynamic center varies with Reynolds number between $0.23c$ and $0.27c$. However, it is encouraging to note from Bertin and Cummings' textbook that the predicted quarter-chord pitching moment is quite close to the pitching moment about the actual aerodynamic center in all the Reynolds number cases depicted in figure 19.

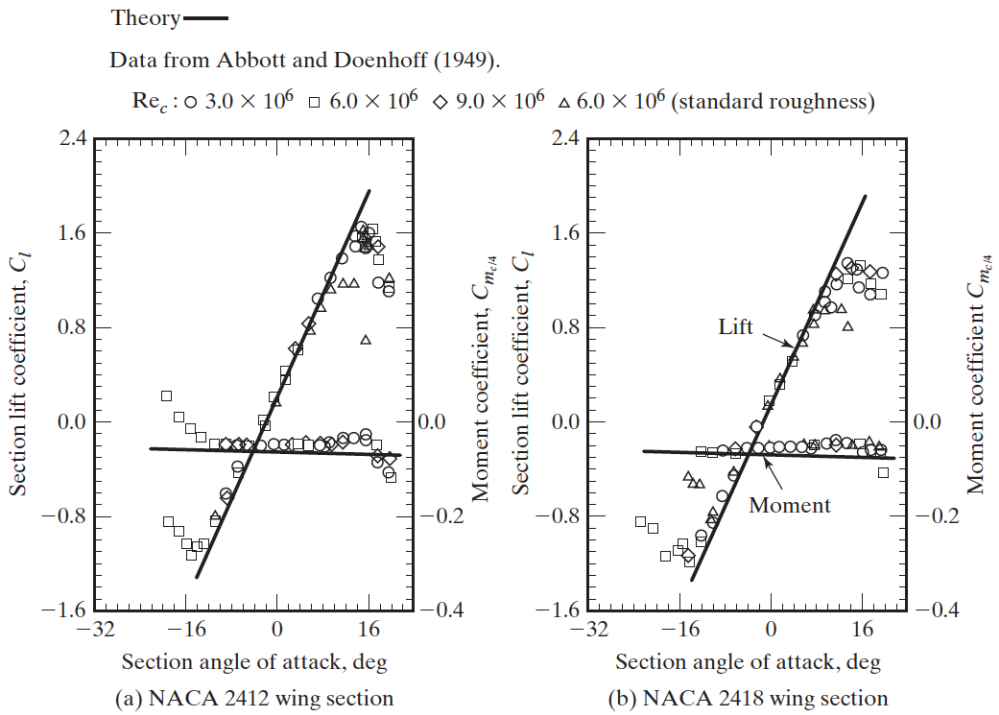

Figure 19: Comparison of the aerodynamic coefficients calculated using thin airfoil theory for two cambered airfoils of different thickness against data from Abbott and von Doenhoff (1949) [adopted from Bertin and Cummings (2013)].

Example 1. Find the dependency of $\alpha_{L=0}$ and $c_{m,c/4}$ of a NACA 4-digit airfoil on the value and chordwise location of its maximum camber from thin-airfoil theory. Hence find these for a NACA 4412 airfoil.

Solution. The camber function of a NACA 4-digit airfoil is

$$\frac{z_c(x)}{c} = \begin{cases} mp^{-2}\left(2px/c - (x/c)^2\right) & \text{for } x \in [0, pc], \\ m(1-p)^{-2}\left(1 - 2p + 2px/c - (x/c)^2\right) & \text{for } x \in [pc, c], \end{cases}$$

where m and p are respectively the value and chordwise location of its maximum camber, both as a fraction of the chord.

The derivative of the camber function is relevant for thin-airfoil theory:

$$\frac{dz_c}{dx} = \frac{d(z_c/c)}{d(x/c)} = 2m(p - x/c) \begin{cases} p^{-2} & \text{for } x/c \in [0, p], \\ (1-p)^{-2} & \text{for } x/c \in [p, 1]. \end{cases}$$

In the transformed coordinates, $x = 0.5c(1-\cos\theta)$ with $\theta_p := \cos^{-1}(1-2p)$, this becomes

$$\frac{dz_c}{dx}(\theta) = m(2p - 1 + \cos\theta) \begin{cases} p^{-2} & \text{for } \theta \in [0, \theta_p], \\ (1-p)^{-2} & \text{for } \theta \in [\theta_p, \pi]. \end{cases}$$

The contribution of camber to the lift coefficient can now be found from eqn (31)

$$c_l = 2\int_0^\pi \frac{dz_c}{dx}(\theta)(\cos\theta - 1)d\theta.$$

Noting the forms of the definite integrals, we first evaluate the following indefinite integral

$$\int (2p - 1 + \cos\theta)(\cos\theta - 1)d\theta = \int \left[\cos^2\theta + (2p-2)\cos\theta + (1-2p)\right] d\theta.$$

We find such integrals of the general form $\int \cos^n\theta d\theta$ in many problems involving polynomial camber functions. These can be solved by integration-by-parts. We note the results for some small values of the integer n below:

$$\int \cos\theta d\theta = \sin\theta, \qquad \int \cos^2\theta d\theta = \frac{1}{2}(\sin\theta\cos\theta + \theta),$$
$$\int \cos^3\theta d\theta = \sin\theta - \frac{1}{3}\sin^3\theta, \qquad \int \cos^4\theta d\theta = \frac{1}{4}\cos^3\theta\sin\theta + \frac{3}{8}(\sin\theta\cos\theta + \theta).$$

Using the above, we have the lift coefficient due to camber alone as

$$\begin{aligned} c_l &= \frac{m}{p^2}\left|\sin\theta\cos\theta + \theta + 4(p-1)\sin\theta + 2(1-2p)\theta\right|_0^{\theta_p} \\ &\quad + \frac{m}{(1-p)^2}\left|\sin\theta\cos\theta + \theta + 4(p-1)\sin\theta + 2(1-2p)\theta\right|_{\theta_p}^{\pi} \\ &= m\frac{(1-2p)\left\{\sin\theta_p\cos\theta_p + 4(p-1)\sin\theta_p + (3-4p)\theta_p\right\} + p^2(3-4p)\pi}{p^2(1-p)^2}. \end{aligned}$$

Recalling that the contribution of angle-of-attack to c_l is $2\pi\alpha$, the zero-lift angle of attack may be found from the above as

$$\alpha_{L=0} = -m\frac{(1-2p)\left\{\sin\theta_p\cos\theta_p + 4(p-1)\sin\theta_p + (3-4p)\theta_p\right\} + p^2(3-4p)\pi}{2\pi p^2(1-p)^2}.$$

We find the pitching moment coefficient about the quarter-chord point for the cambered airfoil from eqn (32):

$$c_{m,c/4} = -\frac{1}{2}\int_0^\pi \frac{dz_c}{dx}(\theta)(\cos\theta - \cos 2\theta)d\theta = -\frac{1}{2}\int_0^\pi \frac{dz_c}{dx}(\theta)(1 + \cos\theta - 2\cos^2\theta)d\theta.$$

As earlier, noting the form of the definite integrals involved, we first evaluate the indefinite integral

$$\begin{aligned} &\int (2p - 1 + \cos\theta)(1 + \cos\theta - 2\cos^2\theta)d\theta \\ &\qquad = \int \left[(2p-1) + 2p\cos\theta + (3-4p)\cos^2\theta - 2\cos^3\theta\right] d\theta \end{aligned}$$

$$= (2p-1)\theta + 2p\sin\theta + \frac{3-4p}{2}(\sin\theta\cos\theta+\theta) - 2\left(\sin\theta - \frac{1}{3}\sin^3\theta\right)$$
$$= 0.5\theta + 2(p-1)\sin\theta + (1.5-2p)\sin\theta\cos\theta + \frac{2}{3}\sin^3\theta,$$

where we have used the above results for $\int \cos^n\theta d\theta$. Putting everything together

$$c_{m,c/4} = -\frac{m}{2p^2}\left|\frac{\theta}{2} + 2(p-1)\sin\theta + \frac{3-4p}{2}\sin\theta\cos\theta + \frac{2}{3}\sin^3\theta\right|_0^{\theta_p}$$
$$- \frac{m}{2(1-p)^2}\left|\frac{\theta}{2} + 2(p-1)\sin\theta + \frac{3-4p}{2}\sin\theta\cos\theta + \frac{2}{3}\sin^3\theta\right|_{\theta_p}^{\pi}$$
$$= -m\frac{(1-2p)\left\{\frac{\theta_p}{2} + 2(p-1)\sin\theta_p + \frac{3-4p}{2}\sin\theta_p\cos\theta_p + \frac{2}{3}\sin^3\theta_p\right\} + \frac{p^2\pi}{2}}{2p^2(1-p)^2}.$$

For a NACA 4412 airfoil, we have $m = 0.04$ and $p = 0.4$, so that $\theta_p = 1.3694$ rad $= 78.463°$. With this, we obtain $\alpha_{L=0} = -0.0725$ rad $= -4.15°$ and $c_{m,c/4} = -0.1062$.

9 Solution of the thickness problem

The thickness problem statement is (see also figure 20): given a freestream speed of V_∞ aligned with a thin symmetric airfoil of thickness function $z_t(x)$, find the density distribution $q(x)$ of the source sheet on the chord line ($z = 0$) such that

$$w(x, 0^\pm) = \pm V_\infty z_t', \qquad x \in (0, c).$$

In Appendix A.1, it has been proved that the sheet-normal velocities above and below a plane source sheet are related to the local source density as $w_u(x) = -w_l(x) = q(x)/2$. Thus, we have the straightforward solution

$$\text{Thickness problem solution:} \qquad q(x) = 2V_\infty z_t'(x), \qquad x \in (0, c). \tag{33}$$

As an aside, it can be verified by integration that the net source strength of the sheet is $2V_\infty[z_t(TE) - z_t(LE)]$. Here, $z_t(LE)$ is zero by definition of the chord line. If the trailing edge is sharp, $z_t(TE)$ also vanishes, thereby ensuring that the source sheet generates a closed streamline (the airfoil body). Evidently, this is not assured when the trailing edge is bluff

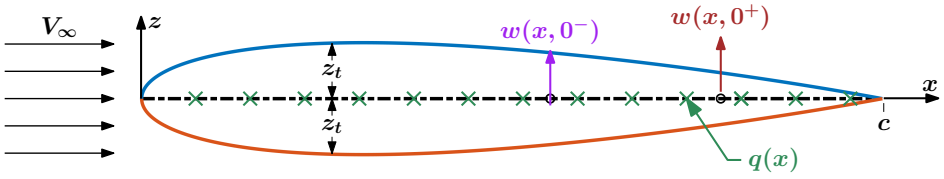

Figure 20: Setup of the thickness problem of thin airfoil theory.

(as in the original NACA 4-digit airfoil geometry), whence the thickness problem will fail to have a meaningful solution.

The sheet-parallel perturbation velocity due to this planar source sheet can be found from the results presented in Appendix A.1. In particular, the $x-$component of velocity just above and below the sheet are

$$u_u(x) = u_l(x) = \frac{V_\infty}{\pi} \int_0^c \frac{z_t'(\zeta)}{x-\zeta} d\zeta. \tag{34}$$

It is unexceptionable that the symmetric airfoil aligned with the freestream has the same perturbation streamwise velocity on both sides.

Using the preceding result in the simplified expression for pressure coefficient c_p derived in eqn (15), the values of c_p on the upper and lower surfaces of the airfoil are found as

$$c_{p,u}(x) = c_{p,l}(x) = -\frac{2}{\pi} \int_0^c \frac{z_t'(\zeta)}{x-\zeta} d\zeta. \tag{35}$$

As expected, there is no pressure difference across the source sheet, so that there is no contribution to lift.

Discussion 1: The integral appearing in eqn (35) (or equivalently in eqn (34)) is *improper* in the sense that the integrand is singular within the range of integration. It turns out that, for most typical thickness distributions, we can still evaluate the integral for almost all x by using the concept of *Cauchy principal value*. This is true even if the airfoil has a rounded leading edge, in which case z_t' is singular at $x = 0$. However, extreme care must be exercised if the integration is to be performed numerically.

Discussion 2: The integration in eqn (35) (or equivalently in eqn (34)) fails to converge at the leading and trailing edges for most typical thickness distributions. However, this is to be expected as these are stagnation points in the aligned flow over a symmetric airfoil, so that $|u| \ll V_\infty$ is a very bad approximation in these cases (u is actually $-V_\infty$ at the stagnation points). Thus, the thickness problem solution should not be trusted very close to the leading and trailing edges, even for arbitrarily thin airfoils.

9.1 Results

Figure 21 presents results of the solution of the thickness problem for two symmetric NACA 4-digit airfoils. Barring the regions near the leading and trailing edges, the pressure coefficient matches well with the results from the more complicated (and accurate) panel method employed for inviscid calculations in XFOIL. The latter simulations were performed at $\alpha = 0$ of course. Discrepancies are somewhat greater for the thicker airfoil, especially near the point of maximum thickness; this is consistent with the relatively greater abuse of the thin-airfoil assumptions thereat.

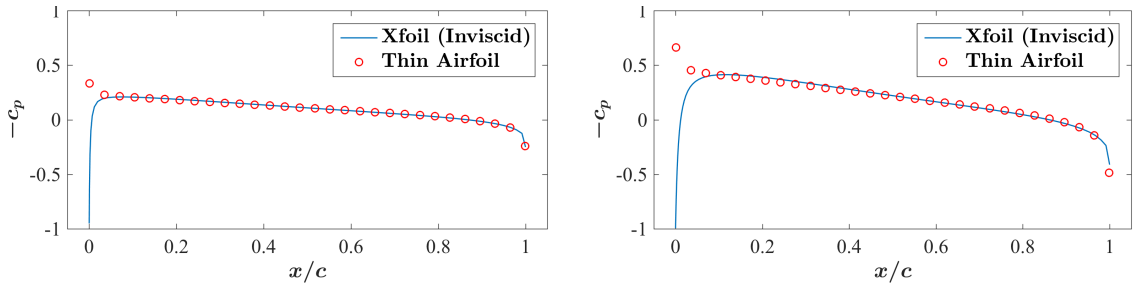

(a) (b)

Figure 21: Comparison of results from thin airfoil theory with those from Xfoil run in inviscid mode for (a) NACA 0006, and (b) NACA 0012 airfoils, both operated at $\alpha = 0$.

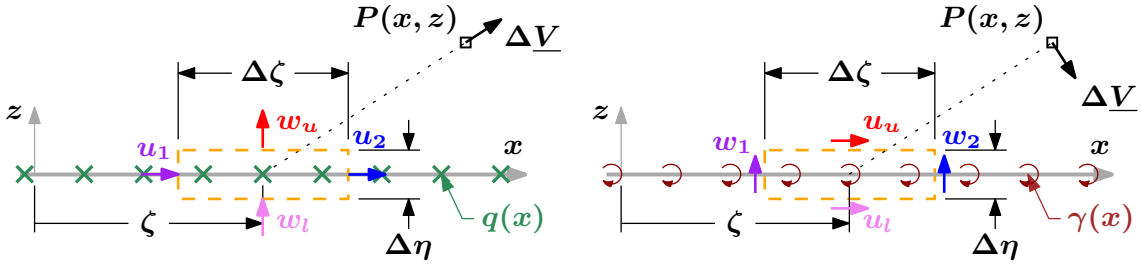

(a) (b)

Figure 22: (a) Planar source sheet of source density $q(x)$. (b) Planar vortex sheet of circulation density $\gamma(x)$.

Appendix

A Analysis of *planar* source and vortex sheets

We specialize the results for general curved sheet singularities discussed in § 3 to plane sheets as shown in figure 22.

A.1 Analysis of a planar source sheet

Consider a planar source sheet along the $x-$axis with source density $q(x)$ (see figure 22a). We have seen in eqn (2) that the differential of local normal (i.e., $z-$component) velocity across a source sheet equals its local source density. In case of a *planar* source sheet, all portions of the sheet other than the local one have zero contribution to the local $z-$velocity; they only generate $x-$velocity on the sheet. That is, $w_u(x)$ and $w_l(x)$ are solely due to $q(x)$. Moreover, from symmetry, they must be equal in magnitude but opposite in sign. Thus,

$$\text{For a planar source sheet:} \qquad w_u(x) = -w_l(x) = \frac{q(x)}{2}. \tag{36}$$

Also, the expression for the velocity at a point $P(x, z)$ due to the planar source sheet

extending from $x = x_1$ to $x = x_2$ (at $z = 0$) is specialized from eqn (3) to

$$\text{For a planar source sheet:} \qquad \underline{V}(x,z) = \frac{1}{2\pi}\int_{x_1}^{x_2} q(\zeta)\frac{(x-\zeta)\hat{\underline{i}} + z\hat{\underline{k}}}{(x-\zeta)^2 + z^2}d\zeta. \tag{37}$$

A.2 Analysis of a planar vortex sheet

Consider a planar vortex sheet along the $x-$axis with circulation density $\gamma(x)$ (see figure 22b). We have seen in eqn (4) that the differential of local tangential (i.e., $x-$component) velocity across a vortex sheet equals its local circulation density. In case of a *planar* vortex sheet, all portions of the sheet other than the local one have zero contribution to the local $x-$velocity; they only generate $z-$velocity on the sheet. That is, $u_u(x)$ and $u_l(x)$ are solely due to $\gamma(x)$. Moreover, from symmetry, they must be equal in magnitude but opposite in sign. Thus,

$$\text{For a planar vortex sheet:} \qquad u_u(x) = -u_l(x) = \frac{\gamma(x)}{2}. \tag{38}$$

Also, the expression for the velocity at a point $P(x,z)$ due to the planar vortex sheet extending from $x = x_1$ to $x = x_2$ (at $z = 0$) is specialized from eqn (5) to

$$\text{For a planar vortex sheet:} \qquad \underline{V}(x,z) = \frac{1}{2\pi}\int_{x_1}^{x_2} \gamma(\zeta)\frac{z\hat{\underline{i}} - (x-\zeta)\hat{\underline{k}}}{(x-\zeta)^2 + z^2}d\zeta. \tag{39}$$

B Alternate way of finding surface normal

A robust method of calculating the unit normal to an arbitrary (three-dimensional) smooth surface is described here. This method can systematically account for the 'outward' vs. 'inward' directions of the normal vector.

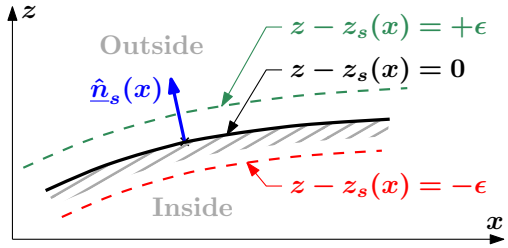

Figure 23: Surface normal calculation from surface gradient.

Consider the surface shown in figure 23, whose equation is $z = z_s(x)$. Define the function

$$\sigma(x,z) := z - z_s(x).$$

For generality, we have allowed the σ to be a function of z also. Note that not only is the equation of the surface $\sigma = 0$, we have also ensured that $\sigma < 0$ *inside* (a body, or a marked domain, say) and $\sigma > 0$ *outside* (the said body or domain). The outward normal points from $\sigma = 0$ to $\sigma > 0$.

It is well known from vector calculus, that gradient of a function f, say, is zero along iso-surfaces of f and is locally normal to an iso-surface pointing in the direction of increasing f. Thus, the unit normal vector to the surface $\sigma = 0$ can be found as

$$\hat{\underline{n}}_\sigma = \frac{\boldsymbol{\nabla}\sigma|_{\sigma=0}}{\|\boldsymbol{\nabla}\sigma|_{\sigma=0}\|}. \tag{40}$$

To evaluate this for the given two dimensional surface, we have

$$\boldsymbol{\nabla}\sigma|_{\sigma=0} = \left[\hat{\underline{k}} - z_s'(x)\hat{\underline{i}}\right]\Big|_{\sigma=0} = -z_s'(x)\hat{\underline{i}} + \hat{\underline{k}},$$

so that

$$\hat{\underline{n}}_\sigma(x) = \frac{-z_s'(x)\hat{\underline{i}} + \hat{\underline{k}}}{\sqrt{1 + (z_s'(x))^2}}. \tag{41}$$

If $|z_s'| \ll 1$, then we have the familiar result

$$\hat{\underline{n}}_\sigma(x) \approx -z_s'(x)\hat{\underline{i}} + \hat{\underline{k}}. \tag{42}$$

It will be recognized that if the body (or demarcated domain) whose surface is under consideration were on the other side of $z = z_s(x)$, then we would have designed the function $\sigma(x, z, z) = z_s(x) - z$. This would have yielded the equal but opposite unit normal vector.